

Numerical modelling of the fracture behaviour of limestone

K.De Proft & W.P.De Wilde

Vrije Universiteit Brussel, Pleinlaan 2, 1050 Brussels, Belgium

M.G.A.Tijssens & L.J.Sluys

Delft University of Technology, Stevinweg 1, 2628 CN, Delft, The Netherlands

ABSTRACT: Numerical simulations of the double-edge notched specimen subjected to tension are performed. The cohesive surface methodology is used for the simulation of the tensile tests. A plasticity law proposed by Carol *et al.* (Carol *et al.* 1997) is introduced as constitutive law for the cohesive surfaces. The influence of the discretisation and of the material parameters defined in the model are studied. Finally, the numerical simulations are compared to the experimentally observed results.

1 INTRODUCTION

In this paper, tensile tests on double-edge notched specimens are analysed experimentally and computationally. The specimens are made of limestone called "Massangis". During experiments both the local, i.e. the crack path, as well as the global response, i.e. load-displacement curve, is recorded. These results are used as verification for numerical simulations performed within the finite element context using the cohesive surface methodology. A plasticity model proposed by Carol *et al.* (Carol *et al.* 1997) is used as the constitutive law for the cohesive surfaces. Also the influence of model parameters and the finite element discretisation is studied.

2 EXPERIMENTAL SET-UP

Rectangular double-edge notched specimens are subjected to a tensile loading. The geometry of the specimens is given in Figure 1. The thickness of the specimen is 11 mm. Two symmetric notches were made in the specimen in order to trigger the fracture process in the middle of the specimens. Two Linear Variable Differential Transducers (LVDT) are used to measure the deformation. These are placed on both sides of the specimen, as shown in Fig. 1. The vertical measuring range of the LVDT's is 20 mm. The average signal of the LVDT is used as the control signal for the test. All tests are performed with displacement control at a rate of 0.3 $\mu\text{m/s}$.

The specimens are glued to the loading platens so that rotation of the boundaries is eliminated.

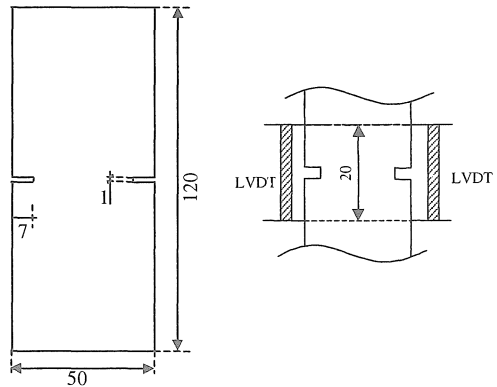


Figure 1. Geometry of the specimens and place of LVDT (All dimensions are in mm)

3 EXPERIMENTAL RESULTS

Some typical load-displacement curves obtained during the experiments are given in Figure 2. After reaching the peak load, the load-displacement curve shows a fast decreasing part, which indicates very brittle behaviour, followed by a smoothly decreasing part.

A typical crack path is shown in Figure 3. It can be seen that only one crack occurs. Crack bridging is not observed during the tests.

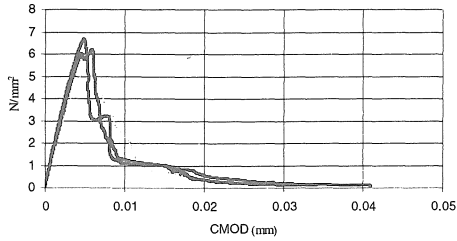


Figure 2. Load-displacement curve

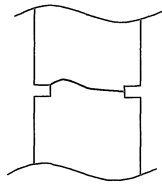


Figure 3. Typical crack path

4 COHESIVE SURFACE MODEL

In the numerical simulations cracking is assumed to start when the stresses in a material point reach the proposed failure surface. Carol *et al.* (Carol *et al.* 1997) proposed a failure surface given in terms of tractions, normal and tangential to a plane with a normal \mathbf{n} :

$$F = T_n - (c - T_n \tan \phi)^2 + (c - f_t \tan \phi)^2 \quad (1)$$

in which $\mathbf{T} = \{T_n, T_t\}$ are the normal and tangential traction, respectively, c is the cohesion, f_t is the tensile strength and ϕ is the angle of internal friction. In the $T_n - T_t$ space, the failure surface has a hyperbolic form. In fact, the failure surface is a smooth version of the combination of a Mohr - Coulomb criterion and a tension cut-off criterion.

The cohesion and the tensile strength control the evolution of the failure surface. These model parameters are a function of the energy dissipated during the fracture process. This energy is defined as:

$$dW_{cr} = T_n d\Delta_n^{cr} + T_t d\Delta_t^{cr} \quad (2a)$$

for tension and

$$dW_{cr} = T_t d\Delta_t^{cr} \left[1 - \left| \frac{T_n \tan \phi}{T_t} \right| \right] \quad (2b)$$

for compression with

$$W_{cr} = \int dW_{cr} \quad (2c)$$

where $d\Delta = \{d\Delta_n^{cr}, d\Delta_t^{cr}\}$ are the normal and the tangential separation of the crack, respectively. For compression, only the shear work, without basic friction, is taken into account.

The tensile strength and the cohesion change with the energy dissipated during fracture according to :

$$f_t = f_{t0} \left(1 - \frac{W_{cr}}{G_{f,I}} \right) \quad (3a)$$

$$c = c_0 \left(1 - \frac{W_{cr}}{G_{f,II}} \right) \quad (3b)$$

where $G_{f,I}$ and $G_{f,II}$ are the mode I and mode II fracture energy respectively, f_{t0} is the initial tensile strength and c_0 is the initial cohesion.

The direction of the inelastic deformations at each point is assumed to be perpendicular to the plastic potential surface. The following non-associative plastic potential is assumed (only the derivatives with respect to the tractions are given since they are used in the computations) :

$$\frac{\partial g}{\partial T_n} = 2 \tan \phi (c_0 - T_n \tan \phi) \quad \text{for } T_n > 0 \quad (4a)$$

$$\frac{\partial g}{\partial T_n} = 2c_0 \tan \left(1 - \frac{T_n}{T_{dil}} \right) \quad \text{for } T_{dil} < T_n < 0 \quad (4b)$$

$$\frac{\partial g}{\partial T_n} = 0 \quad \text{for } T_n < T_{dil} \quad (4c)$$

$$\frac{\partial g}{\partial T_t} = 2T_t \quad (4d)$$

For numerical reasons, a transition area between 0 and T_{dil} is defined for the derivative with respect to the normal traction. When the normal tractions is smaller than T_{dil} , dilatancy is not taken into account.

The total deformation can be split up into an elastic and a plastic (cracked) part :

$$d\Delta_i = d\Delta_i^{el} + d\Delta_i^{cr} \quad (i = n, t) \quad (5)$$

The plastic deformation is defined as :

$$d\Delta_i^{cr} = \lambda \frac{\partial g}{\partial T_i} \quad (i = n, t) \quad (6)$$

where λ is the plastic multiplier. The plastic multiplier can be obtained by the consistency equation, i.e. $dF = 0$. The rate equations are obtained following the classical elasto-plastic theory. The integration of the rate equations is done using an implicit Euler backward scheme (Crisfield. 1991).

5 THE COHESIVE SURFACE METHODOLOGY

The numerical simulations are performed within the finite element context. Cohesive surfaces are embedded in the continuum and are discretised separately as was first proposed by Xu and Needleman (Xu and Needleman, 1994). Separate constitutive laws are defined for the surfaces and the continuum.

5.1 Numerical implementation

Although large strains are not expected in the bulk, finite strain effects may be important in the neighbourhood of crack tips. Therefore finite strains are taken into account in the continuum, using a Total Lagrangian description for which the incremental equilibrium equations are specified through the rate form of the principle of virtual work :

$$\begin{aligned} \Delta t \int_V (\tau^{ij} \delta \eta_{ij} + \tau^{ik} u_{,k}^j \delta u_{,j,i}) dV + \Delta t \int_{S_i} T_\alpha \delta \Delta_\alpha dS_i = \\ \Delta t \int_{S_u} i^i \delta u_i dS_u - \\ \left[\int_V \tau^{ij} \delta \eta_{ij} dV + \int_{S_i} T_\alpha \delta \Delta_\alpha dS_i - \int_{S_u} i^i \delta u_i dS_u \right] \quad (\alpha = n, t) \end{aligned} \quad (7)$$

in which Δt is the time increment, V is the volume and S_u is the outer surface of the body in the reference configuration and S_i is the current internal cohesive surface. The latter is the collection of all the cohesive surfaces embedded in the continuum. The term between brackets is the equilibrium correction, which prevents drifting of the solution from the true equilibrium path. This drifting can occur due to the finite time increments used in the explicit time integration scheme. For equilibrium, this term equals zero.

For the continuum elements, elastic behaviour is assumed and is introduced through a hypo-elastic constitutive law in terms of the Second order Piola-Kirchhoff stress $\tau = \tau^{ij} e_i e_j$ and the Lagrangian strain $\eta = \eta_{ij} e^i e^j$:

$$\dot{\tau}^{ij} = \mathcal{L}^{ijkl} \dot{\eta}_{kl} \quad (8)$$

in which \mathcal{L}^{ijkl} is the material modulus tensor, which is expressed in terms of Young's modulus E and Poisson's ratio ν for an isotropic material.

5.2 Indirect displacement control

In this paper, the cohesive surface methodology is used to describe fracture in a double-edge notched (DEN) tensile bar. Because these experiments show a snap-back behaviour with respect to the applied loading, an Indirect Displacement Control technique (de Borst, 1987) is used.

The set of equations can be rewritten as :

$$\begin{bmatrix} K_{ff} & K_{fp} \\ K_{pf} & K_{pp} \end{bmatrix} \begin{bmatrix} \Delta Q_f \\ \Delta Q_p \end{bmatrix} = \begin{bmatrix} \Delta F_f \\ 0 \end{bmatrix} + \begin{bmatrix} R_f \\ R_p \end{bmatrix} \quad (9)$$

in which ΔQ_f and ΔQ_p are the free and prescribed degrees of freedom respectively. ΔF_f is the incremental external force and R_f and R_p contain the equilibrium correction and the reaction forces respectively.

A load factor Δs is defined so that

$$\Delta F_f = \Delta s \hat{F}_f, \quad \Delta Q_p = \Delta s \hat{Q}_p \quad (10)$$

where $\|\hat{F}_f\| = 1$ and $\|\hat{Q}_p\| = 1$. The solution is obtained as

$$\Delta Q_f = \Delta s Q_f^I + Q_f^{II} \quad (11)$$

in which $Q_f^I = K_{ff}^{-1} \{ \hat{F}_f - K_{fp} \hat{Q}_p \}$ and $Q_f^{II} = K_{ff}^{-1} R_f$.

The load factor Δs is obtained by controlling the increase of the average crack opening displacement of the notches, i.e.

$$CMOD = \frac{1}{2} \left[(\Delta Q_{f,y}^A - \Delta Q_{f,y}^B)_{left} + (\Delta Q_{f,y}^A - \Delta Q_{f,y}^B)_{right} \right]$$

as explained in Figure 4.

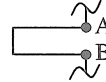


Figure 4. Nodes for indirect displacement control

6 NUMERICAL RESULTS

The geometry, shown in Fig. 1 is used in the numerical simulations. Due to the limited thickness, a 2D model is used. Plane strain conditions are assumed. Rotation of the boundaries is restricted.

6.1 Influence of the discretisation

The influence of the discretisation is studied by using three different meshes, as shown in Fig. 5. For every mesh, an analysis is performed with the following model parameters: tensile strength $f_t = 6.2$ MPa, cohesion $c = 10$ MPa, internal friction angle $\varphi = 0.46$ rad, mode-I fracture energy $G_{f,I} = 0.035$ N/mm and mode-II fracture energy $G_{f,II} = 0.15$ N/mm. The Young's Modulus is taken $E = 41.9$ GPa and Poisson's ratio $\nu = 0.25$. These values resulted in the best fit for the different meshes.

The resulting crack paths are shown in Fig. 5. The load displacement curves are given in Fig. 6.

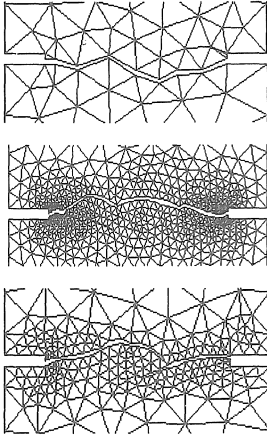


Figure 5. Crack path for mesh 1, mesh 2 and Mesh3

As can be seen in Fig. 5, the fracture paths for the different meshes are similar and resemble the experimentally obtained crack path (see Fig. 3). Because fracture can only occur following the finite element boundaries, a slight mesh dependence is introduced with respect to the crack path, but not with respect to the size of the finite element. The location and the path of the crack are unrestricted, since the crack can propagate along every finite element edge.

When the load displacement curves are studied, small differences (within 7%) in peak load are observed. The post peak behaviour is a little bit underestimated. It can be concluded that, when the cohesive surfaces are scattered throughout the volume randomly, i.e. the surfaces have random inclinations, the methodology has good predictive capabilities.

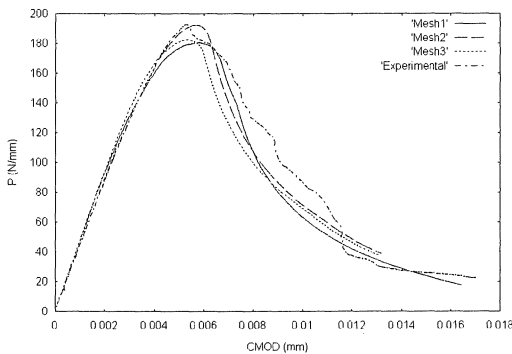


Figure 6. Load displacement curve for different meshes

6.2 Influence of the model parameters

Finally, the influence of the model parameters is studied. For every mesh used in the previous section, the model parameters are changed.

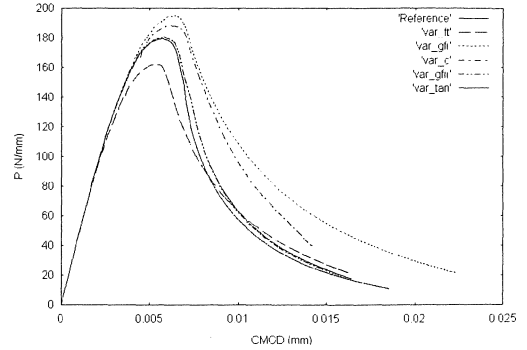


Figure 7. Influence of model parameters for mesh 1

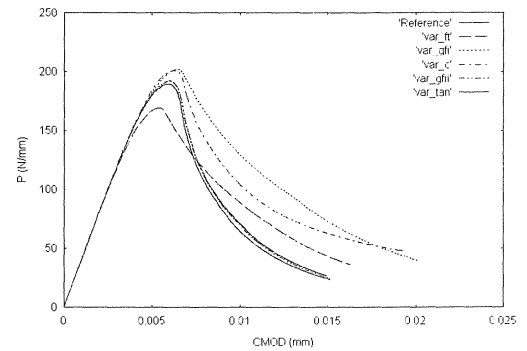


Figure 8. Influence of model parameters for mesh 2

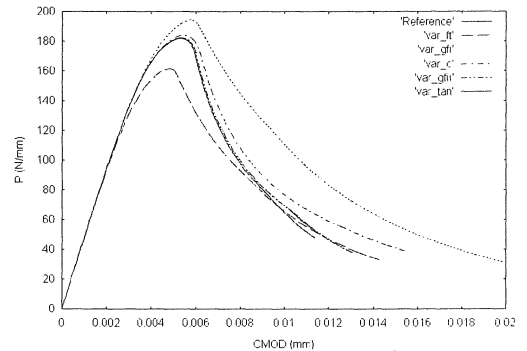


Figure 9. Influence of model parameters for mesh 3

The most important influence is observed for the tensile strength and the mode-I fracture energy. This was expected since the test was a mode-I fracture test. It can be seen that for the three meshes a lower tensile strength results in a lower peak. For a decrease of 15% for the tensile strength, the decrease of the peak load is about 10%. When the mode-I fracture energy is increased, the area below the load

displacement curve also increases, resulting in a less steep descending branch. Also the peak load is affected. An increase of the mode-I fracture energy with 40 % results in an increase of the peak load of 6 %.

The influence of the mode-II fracture energy and the internal friction angle is negligible. The variation of the peak load is within 1 %. Sometimes, little differences in the tail of the post peak behaviour are observed.

A remarkable result is obtained by varying the cohesion. In every example, the cohesion is increased from a value $c = 10$ Mpa to $c = 30$ Mpa. For mesh 1, this increase results in an increase of the peak load of 4 %. For mesh 2 a comparable result is found. For mesh 3, a negligible increase of peak load is found (within 1%).

The variation of peak load, as a consequence of an increased cohesion, can be seen as a result from the methodology. Since the crack only can propagate following finite element boundaries, the different meshes can result in a different peak load.

When we analyse the post peak behaviour, we observe that every tail of the load displacement curves are affected when the cohesion is increased. For mesh 2, an explanation can be found in the crack path. Figure 10 shows that there is no unique crack path, but different smaller cracks. One can even observe bridging. This results in higher energy dissipation during the fracture process and explains the more ductile response.

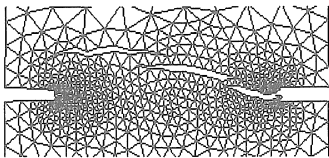


Figure 10. Crack path for mesh 2 with increased cohesion

It should also be noted that for mesh 2, most of the cracked cohesive surfaces are horizontal. In an inclined cohesive surface, both a normal and tangential component of the traction is present. When the cohesion is bigger, it takes longer to reach the cracking surface as shown in Fig. 11. For mesh 2, the surfaces between the cracks are almost vertical, so a bigger load would be necessary to crack the surfaces. This explains the bridging. This phenomenon also results in a higher energy dissipation, and thus a more ductile response in the post peak behaviour.

It is clear that in this case the result is somewhat mesh dependent. As a consequence, a good choice of the model parameters is very important.

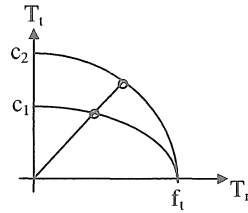


Figure 11. Influence of bigger cohesion in yield surface

7 CONCLUSIONS

In this paper, the cohesive surface methodology is used for the simulations of double edge notched tensile tests. The material law proposed by Carol *et al.* (Carol *et al.*, 1997) was used as a constitutive law in the cohesive surfaces.

In a first set of simulations, the influence of the discretisation was studied. It was shown that the influence of the discretisation could not be ruled out completely. However the different responses for the different meshes showed a similar behaviour, and only small differences were found in peak load and post peak behaviour.

Then the influence of the model parameters was studied. It was shown that for a mode-I test, the tensile strength and the mode-I fracture energy are the most important parameters. The influence of varying the cohesion depends on the discretisation used.

Generally, it can be concluded that the mesh is very important. For the simulation of fracture, the mesh must be fine enough and random, as already pointed out by Tijssens *et al.* [Tijssens *et al.* 2000]. This means that the inclination of the cohesive surfaces must be randomly chosen. In this way, the mesh resembles the microstructure of the material and the best results can be obtained.

REFERENCES

- [1] I. Carol, C.M. López, P.C. Prat., 1997, Normal/Shear Cracking model : Application to Discrete Crack Analysis. *Journal of Engineering Mechanics*, 123(8): 765-773..
- [2] M.Crisfield, 1991, *Non-linear finite element analysis of solids and structures*. Volume I. John Wiley & Sons, Inc., New York, N.Y.
- [3] X.-P. XU and A. Needleman, 1994, Numerical Simulations of Fast Crack growth in Brittle Solids. *J. Mech. Phys. Solids*, 42(9):1397 -1434.
- [4] de Borst R., 1987, Computation of post-bifurcation and post-failure behaviour of strain-softening solids. *Computers & Structures*, 25, 211-224.
- [5] Tijssens M.G.A., Sluys L.J., van der Giessen E., 2000, Numerical simulation of quasi-brittle fracture using damaging cohesive surfaces. *Eur. J. Mech. A/Solids*, 19,761-779.

